A comparison of one-dimensional traveling waves in inverse and normal fluidized beds

Maureen A. Howley
Otto H. York Department of Chemical Engineering
New Jersey Institute of Technology, Newark, NJ 07102

Benjamin J. Glasser
Department of Chemical and Biochemical Engineering
Rutgers University, Piscataway NJ 08854

Abstract

The state of uniform fluidization is usually unstable to small disturbances, and this can lead to the formation of vertically traveling voidage waves. In inverse fluidization, when particle density is less than fluid density ($\rho_s < \rho_f$), particles fluidize in the direction of gravity when the drag force exerted by the fluid overcomes buoyancy. Inverse fluidization thus provides a unique parameter space, which augments the study of instability behavior in normal fluidization when $\rho_f < \rho_s$. Using continuum equations of continuity and motion, we compared the linear stability of normal and inverse bed modes to examine the effect of the Froude number (Fr) and fluid to solid density ratio ($\delta = \rho_f/\rho_s$). Making use of numerical bifurcation analysis and continuation, periodic solutions in the form of one-dimensional traveling waves (1D-TWs) were computed. Based on wave growth rates and bifurcation structure, we identified the Fr as an important parameter for predicting instability *strength*. However, δ affects instability *onset*, or the point at which the base state is rendered unstable. In the case studies we examined, traveling waves were shown to propagate in the direction of fluidization, and asymmetrical, high amplitude 1D-TW profiles suggest fully developed bubble-like structures are oriented in the direction of fluidization.

1 Introduction

In inverse fluidization, low density particles become mobile, or *fluidize*, when the drag exerted by a heavier fluid flowing downwards through the column overcomes the buoyancy force on the particles (Gőz, Glasser, Kevrekidis & Sundaresan [1]). Inverse fluidization is the reverse of what is considered to be normal fluidization, where heavier particles are fluidized by the upwards flow of a lighter gas or liquid. Fluidizing lightweight particles by a heaver medium is advantageous in many important industrial applications where enhanced multi-phase mixing can improve heat and mass transfer performance (see Muroyama & Fan [2]). For example, in biotechnology and catalytic chemical reaction engineering, inverse turbulent three-phase reaction systems have been investigated for improved selectivity and yield. In these systems, lightweight particles are fluidized by the countercurrent flow of liquid downwards and gas bubbles upwards (Fan, Muroyama & Chern [3]; Krishnaiah, Guru & Sekar [4]; Comte, Bastoul, Hebrard, Roustan & Lazarova [5]). In fluidized-bed dry particle coating, a high-density super critical fluidization medium (operating in inverse mode) may improve coating efficiency by affecting the frequency and impact value of particle-particle collisions. However, it is difficult to support the use of this mode as a viable alternative without a a better understanding of how fluidization *direction* (relative to gravity) affects instability behavior in the bed.

In normal fluidized beds, it has been well-documented that the base-state of uniform fluidization is usually unstable to small disturbances, and this can lead to the formation and propagation of vertically traveling *voidage waves*. When primary instabilities becomes spatially amplified in the bed, this can bring about complex bubbling and turbulent flow regimes, which completely alter the flow characteristics of the system (Gibilaro [6]). In gas-fluidized beds, voidage waves are in the form of *bubbles*, where experimental evidence has shown that just beyond conditions of minimum fluidization, the solids tend to remain compacted as increasing volumes of gas pass through the condensed phase "much in the manner of a gas passing through an actual liquid" (Wilhelm & Kwauk [7]). This mode of fluidization is often referred to as *aggregative*, and differs dramatically from flow behavior that is sometimes observed in liquid-fluidized beds, which expand uniformally and are generally more stable in operation (referred to as non-bubbling or *particluate*).

In the fluidization research, *two-phase* continuum models have been used to study the stability behavior of gas- and liquid-fluidized beds. This approach uses *ensemble*- or volume-averaged equations of continuity and motion to describe the behavior of the fluid and particle phases using constitutive relationships or closure laws to express the various force terms as functions of locally averaged variables. Researchers have generally adopted closures based on empirical correlations (Pigford & Baron [8]; Murray [9]; Anderson & Jackson [10]; Garg & Pritchett [11]), but constitutive terms have also been theoretically derived using physical arguments (Batchelor [12]), and from first principles (Koch & Sangani [13]). Anderson, Sundaresan & Jackson [14] successfully demonstrated that these equations do capture the physics necessary to distinguish between bubbling and non-bubbling systems. Recently, Duru, Nicolas, Hinch & Guazzelli [15] tested this approach experimentally by relating the physical properties of saturated voidage waves to the particle phase pressure and viscosity terms. Their results confirmed that the model was satisfactory for describing the behavior of one-dimensional voidage waves within the experimental parameter range investigated (see also Duru & Guazzelli [16]).

In the experimental work of Wilhelm & Kwauk [7], solid-air (or aggregative) systems were found to be separable from solid-water (or particulate) systems on the basis of the dimensionless Froude number evaluated at minimum fluidization velocity, for a wide range of particle species. Experimental evidence of such distinct flow behavior has prompted its investigation by linear stability analysis of the uniform fluidization state. In a stability analysis of gas- and liquid-fluidized beds, Gőz [17, 18] analyzed primary bifurcations of two-dimensional vertically and oblique traveling waves from the base-state, and found only minor differences between gas- and liquid-fluidized beds. Gőz [19] also found similar bifurcation structure exhibited in gas- and liquid-fluidized beds having small Fr approximations. Gőz & Sundaresan [20] extended a previous analysis performed by Gőz [21], to examine the stability of one-dimensional periodic waves to two-dimensional perturbations of large transverse wavelength in liquid-fluidized beds by considering the effects of fluid phase inertia and viscosity. These authors demonstrated that the instability mechanism is the same for both gas- and liquid-fluidized beds, and concluded that scaling differences play an important role in distinquishing the difference in gas- and liquid-fluidized bed behavior, *viz.* the Fr number group.

Linear stability analyses of the base state have since led to the computation of fully-developed, one and two-dimensional traveling wave solutions using numerical simulation techniques and bifurcation theory (Glasser, Kevrekidis & Sundaresan [22]). These authors found that for both gas- and liquid-fluidized beds, two-dimensional traveling waves were subsequently born out of one dimensional traveling wave solutions emerging through Hopf bifurcations of the steady state solution. Glasser, Kevrekidis & Sundaresan [23] proposed that a distinction between bubbling and non-bubbling flow behavior can be made based upon an examination of the particle-phase velocity field in high-amplitude two-dimensional traveling wave solutions. By examining a wide range of parameter values, these authors demonstrated that the potential for bubbling is dictated by the dimensionless quantity Ω where Ω^2 is shown to be equivalent to Fr by adopting a natural scale for the particle phase viscosity.

In this paper, a comparative linear stability analysis of the uniform fluidization state is carried out in inverse and normal systems to determine if the role of the Fr in distinguishing bubbling from non-bubbling bed behavior is consistent with the ideas put forth previously by other researchers. The inverse liquid bed proves to be an important case study because it introduces an additional dimensionless parameter set having values, which do not exist within the set defined by normal fluidization. Moreover, the role of fluidization *direction* (with respect to gravity) can be critically examined. We compared instability behavior in normal and inverse liquid beds for systems having comparable Fr numbers and for systems having Fr numbers, which differed by a factor of 4. Linear stability is analyzed at the *marginal* stability point, or point at which both systems are rendered unstable at an expanded bed volume defined by some critical solids volume fraction ϕ_c. High amplitude one-dimensional traveling wave solutions are used to compare the structure and propagation behavior of wave forms in the two beds.

Volume averaged equations of continuity and motion from the theory of Anderson & Jackson [10] are presented and discussed in Section 2. In Section 3, the linear stability of the uniformly fluidized base state is examined in normal and inverse bed modes, and one-dimensional traveling wave solutions are computed in Section 4 using a derivation from the work of Needham & Merkin [24]. Results are presented in Section 5 for water-fluidized systems using the two-fluid model to examine the effect of the dimensionless Fr number and δ. Conclusions are discussed in Section 6.

2 Equations of motion

We begin with a description of the volume-averaged equations of continuity and motion for a two-phase system consisting of a fluid and solid phase [10]. These equations have been written in a moving frame of reference at constant velocity ω (Gőz [25]), and take the form:

$$\frac{\partial \epsilon}{\partial t} + \nabla \cdot [\epsilon\ (\mathbf{u} - \omega \mathbf{k})] = 0 \tag{1}$$

$$\frac{\partial \phi}{\partial t} + \nabla \cdot [\phi\,(\mathbf{v} - \omega \mathbf{k})] = 0 \tag{2}$$

$$\rho_f \epsilon \left[\frac{\partial \mathbf{u}}{\partial \mathrm{t}} + (\mathbf{u} - \omega \mathbf{k}) \cdot \nabla \mathbf{u}\right] = -\epsilon \nabla \cdot \boldsymbol{\sigma}_f - \tilde{\mathbf{F}} + \epsilon \rho_f \mathbf{g} \tag{3}$$

$$\rho_s \phi \left[\frac{\partial \mathbf{v}}{\partial \mathrm{t}} + (\mathbf{v} - \omega \mathbf{k}) \cdot \nabla \mathbf{v}\right] = -\phi \nabla \cdot \boldsymbol{\sigma}_f - \nabla \cdot \boldsymbol{\sigma}_s + \tilde{\mathbf{F}} + \phi \rho_s \mathbf{g} \tag{4}$$

where ϕ is the local mean solids volume fraction, ϵ is the local mean bed voidage ($\epsilon = 1 - \phi$), and ρ_f and ρ_s are the fluid and solid phase densities respectively. The locally averaged interstitial fluid velocity and particle phase velocity vectors are written in the laboratory frame of reference as $\mathbf{u}$ and $\mathbf{v}$ respectively. The fluid and solid phase stress tensors (defined in a compressive sense) are represented by $\boldsymbol{\sigma}_f$ and $\boldsymbol{\sigma}_s$. The gravity force vector is $\mathbf{g}$, and $\mathbf{k}$ is the unit vector pointing in the positive vertical direction against gravity. $\tilde{\mathbf{F}}$ represents the fluid-particle interative force per unit of bed volume, which results from the relative motion of the fluid and particle phases. Writing the equations in this way introduces the wavespeed ω, which is used in this analysis as a bifurcation parameter.

The fluid phase stress tensor is represented by $\boldsymbol{\sigma}_f$ and is, in general, a function of the rate of deformation of the fluid phase. A form analogous to a Newtonian fluid will be assumed for the fluid phase stress tensor [10]:

$$\boldsymbol{\sigma}_f = P\boldsymbol{I} - \mu\left[\nabla\mathbf{u} + \nabla(\mathbf{u})^T - \Big(\frac{2}{3} - \frac{\lambda}{\mu}\Big)(\nabla\cdot\mathbf{u})\,\boldsymbol{I}\right] \tag{5}$$

where P is the fluid pressure, and μ and λ are the fluid shear and bulk viscosities respectively. For the particle phase, continuum mechanics arguments provide a constitutive relation for $\boldsymbol{\sigma}_s$ in terms of the rate of deformation of the particle phase (Anderson & Jackson [26]). The particle phase stress tensor takes the form:

$$\boldsymbol{\sigma}_s = P_s\boldsymbol{I} - \mu_s\left[\nabla\mathbf{v} + \nabla(\mathbf{v})^T - \Big(\frac{2}{3} - \frac{\lambda_s}{\mu_s}\Big)(\nabla\cdot\mathbf{v})\,\boldsymbol{I}\right] \tag{6}$$

where P_s is the solid phase pressure, and μ_s and λ_s are the effective shear and bulk viscosities respectively. In this study, we have adopted a closure from the work of Johnson & Jackson [27] for expressing P_s as a monotonically increasing function with respect to solids volume fraction ϕ:

$$P_s = \frac{g_o\phi^{m_1}}{(\phi_p - \phi)^{m_2}} \tag{7}$$

where g_o is a constant, and ϕ_p represents the solids volume fraction under close-packed conditions ($\phi_p = 0.65$, Berryman [30]). We have considered both a linear form for P_s ($m_1 = 1$ and $m_2 = 0$) and a non-linear form ($m_1 = 1$ and $m_2 = 2$) [22]. The shear viscosity of the solid μ_s is expected to be a monotonically increasing function with respect to ϕ [22]:

$$\mu_s = \frac{R\phi}{1 - (\phi/\phi_p)^{1/3}} \tag{8}$$

where the value of parameter R is selected to yield a shear viscosity within a range suggested by experiments. The bulk viscosity is assumed to be zero ($\lambda_s = 0$) in this study [26].

The force due to the relative motion of the fluid and solid ($\tilde{\mathbf{F}}$) consists of a frictional or "drag" force in the direction of fluid flow, which is a function of slip velocity between the particles and fluid, and a force of virtual mass, which is a function of the acceleration reaction of fluidized particles induced by a change in fluid phase momentum. We have adopted a general closure from [26] to express this force term:

$$\tilde{\mathbf{F}}_i = \epsilon\beta\,(\mathbf{u} - \mathbf{v}) + \phi\mathbf{C}\rho_f\frac{\mathrm{d}\,(\mathbf{u} - \mathbf{v})}{\mathrm{dt}}. \tag{9}$$

The first term on the right hand side of equation 9 represents the drag on the particles due to the flow of fluid where β is the drag coefficient. A convenient form for a monocomponent bed is the Richardson & Zaki relation [28], which expresses the interstitial fluid velocity in the vertical z direction (u_z) as a function of bed expansion ϕ:

$$u_z = v_t\,(1 - \phi)^{(n-1)} \tag{10}$$

In this expression, v_t is the terminal settling velocity (normal bed mode) or rising velocity (inverse bed mode) of a single particle in an infinite fluid medium. The empirical correlation index (n) is a function of the local voidage and particle Reynolds number Re computed at v_t [28]. The settling (or rising) velocity is computed under equilibrium conditions when a single sphere is allowed to settle by gravity (when $\rho_s > \rho_f$), or rise by buoyancy (when $\rho_s < \rho_f$) in a viscous fluid at constant velocity. The drag force coefficient (in expression 9), derived from the Richardson–Zaki relation for a uniformly fluidized bed, is written as,

$$\beta = \frac{\phi\left(\rho_s - \rho_f\right) g_z}{v_t\left(1-\phi\right)^{(n-1)}} \tag{11}$$

where g_z is the standard acceleration of gravity. Using the particle Reynolds number defined as,

$$Re = \frac{2 r_p v_t \rho_f}{\mu} \tag{12}$$

v_t is computed using the equilibrium force balance relationship:

$$F_D + F_B = F_G \tag{13}$$

where F is the force per unit volume exerted on a single spherical particle of radius r_p, and subscripts D, B and G represent 'drag', 'buoyancy', and 'gravity' respectively. The individual force expressions are written as,

$$\begin{aligned} F_D &= \frac{\pi}{2}\rho_f v_t^2 r_p^2 \beta_D && (14)\\ F_B &= +\frac{4\pi}{3}\rho_f r_p^3 g_z && (15)\\ F_G &= -\frac{4\pi}{3}\rho_s r_p^3 g_z && (16) \end{aligned}$$

The case studies examined in this work fall within the intermediate flow regime defined by $1 \le Re \le 10^3$ where the drag coefficient β_D in equation 14 is estimated by $\beta_D \approx 18 Re^{-0.6}$ (Denn [29]). Using the force balance relationship (equation 13), v_t can be estimated by,

$$v_t \approx \left[\frac{2 g_z}{27}\left(\frac{\rho_s}{\rho_f} - 1\right)\right]^{5/7} \left(2 r_p\right)^{8/7} \left(\frac{\rho_f}{\mu}\right)^{3/7} \tag{17}$$

Hence the terminal velocity (normal mode) is positive, and the rising velocity (inverse mode) is negative due to the sign of the term $(\rho_s/\rho_f - 1)$.

The second term on the right hand side of equation 9 represents the force of virtual mass, which is considered to be important in liquid-fluidized beds. $\mathbf{C}$ is the virtual mass coefficient. The relative acceleration rate takes the following form [26]:

$$\frac{\mathrm{d}\left(\mathbf{u}-\mathbf{v}\right)}{\mathrm{dt}} = \frac{\partial}{\partial t}\left(\mathbf{u}-\mathbf{v}\right) + \mathbf{v}\cdot\nabla\left(\mathbf{u}-\mathbf{v}\right)$$

3 Linear stability analysis

The simplest solution to the model equations 1 through 4 represents that of the uniform fluidization state where; the local mean particle velocity vector, $\mathbf{v}$ is zero; the local mean fluid velocity vector, $\mathbf{u}$ is constant in space and time and directed in either the positive or negative vertical direction depending on the term $(\rho_s/\rho_f - 1)$ in equation 17; and the local mean solids volume fraction, ϕ is spatially uniform and constant in time. Under these conditions,

$$\phi = \phi_o \tag{18}$$

$$\epsilon = \epsilon_o = (1 - \phi_o) \tag{19}$$

$$\mathbf{u} = \pm \mathbf{k} u_o \tag{20}$$

$$\mathbf{v} = \mathbf{0} \tag{21}$$

where the subscript 'o' is used to indicate that a quantity is evaluated at conditions corresponding to the uniform base state. In the absence of velocity gradients, all inertial and viscous force terms reduce to zero. Moreover, the bed is considered homogeneous with respect to the locally averaged particle concentration $\rho_s\phi_o$. As a result, the gradient of the isotropic compressive force term (∇P_s) also goes to zero, and the pressure gradient across the bed is due only to the dynamic fluid pressure in the direction of fluid velocity. Since we are interested in the stability of the uniform base state, we impose a perturbation in the form of a localized voidage disturbance having small amplitude, and rewrite the equations in terms of perturbation variables $\phi\prime$, $\epsilon\prime$, $\mathbf{u}\prime$, $\mathbf{v}\prime$ and $P\prime$, which are defined as,

$$\phi = \phi_o + \phi\prime \tag{22}$$

$$\mathbf{u} = \pm \mathbf{k} u_o + \mathbf{u}\prime \tag{23}$$

$$\mathbf{v} = \mathbf{0} + \mathbf{v}\prime \tag{24}$$

$$P = P_o + P\prime \tag{25}$$

The equations are linearized about the uniform base state by substituting the above expressions for ϕ, ϵ, $\mathbf{u}$, $\mathbf{v}$ and P (equations 22 through 25) into equations 1 through 4, and performing a Taylor series expansion about the steady state solution. Neglecting terms in the series involving powers greater than one, and elimating products of perturbation variables results in a system of linearized partial differential equations (PDEs) written in one-dimension z as,

$$\frac{\partial \epsilon\prime}{\partial t} + \epsilon_o \nabla \cdot \mathbf{u}\prime + (u_o - \omega)\, \mathbf{k} \frac{\partial \epsilon\prime}{\partial z} = 0 \tag{26}$$

$$\frac{\partial \phi\prime}{\partial t} + \phi_o \nabla \cdot \mathbf{v}\prime - \omega \mathbf{k} \frac{\partial \phi\prime}{\partial z} = 0 \tag{27}$$

$$\rho_f \left(1 + \frac{\phi_o C_o}{(1-\phi_o)}\right) \left[\frac{\partial \mathbf{u}\prime}{\partial \mathrm{t}} + (u_o - \omega)\, \mathbf{k} \frac{\partial \mathbf{u}\prime}{\partial \mathrm{z}}\right] - \frac{\phi_o C_o \rho_f}{(1-\phi_o)} \left[\frac{\partial \mathbf{v}\prime}{\partial \mathrm{t}} - \omega \mathbf{k} \frac{\partial \mathbf{v}\prime}{\partial \mathrm{z}}\right] = \tag{28}$$

$$-\nabla \cdot P\prime + (\lambda_o + 1/3\mu_o)\, \nabla (\nabla \cdot \mathbf{u}\prime) + \mu_o \nabla^2 \mathbf{u}\prime - \beta_o (\mathbf{u}\prime - \mathbf{v}\prime) - \beta\prime_o \phi\prime u_o \mathbf{k}$$

$$\left(\rho_s \phi_o + \frac{\phi_o C_o \rho_f}{(1-\phi_o)}\right) \left[\frac{\partial \mathbf{v}\prime}{\partial \mathrm{t}} - \omega \mathbf{k} \frac{\partial \mathbf{v}\prime}{\partial \mathrm{z}}\right] - \rho_f \phi_o \left(1 + \frac{C_o}{(1-\phi_o)}\right) \left[\frac{\partial \mathbf{u}\prime}{\partial \mathrm{t}} + (u_o - \omega)\, \mathbf{k} \frac{\partial \mathbf{u}\prime}{\partial \mathrm{z}}\right] = \tag{29}$$

$$-P\prime_{so} \nabla \cdot \phi\prime + (\lambda_{so} + 1/3\mu_{so})\, \nabla (\nabla \cdot \mathbf{v}\prime) + \mu_{so} \nabla^2 \mathbf{v}\prime + \beta_o (\mathbf{u}\prime - \mathbf{v}\prime) + \beta\prime_o \phi\prime u_o \mathbf{k} - \phi\prime (\rho_s - \rho_f)\, g_z \mathbf{k}$$

where the terms $\beta\prime_o$ and $P\prime_{so}$ are used to represent the following derivatives evaluated under conditions of uniform fluidization:

$$\beta\prime_o = \left(\frac{\partial \beta}{\partial \phi}\right)_{\phi=\phi_o} \qquad P\prime_{so} = \left(\frac{\partial P_s}{\partial \phi}\right)_{\phi=\phi_o}$$

These equations have been made non-dimensional by taking the particle radius r_p as a length scale, and the interstitial fluid velocity at uniform fluidization in the axial direction $\pm(u_{zo})$ as a velocity scale computed using the Richardson & Zaki form. Hence, in normal mode operation, fluid velocity is in the positive vertical z direction $(+u_{zo})$ and in the direction of gravity $(-u_{zo})$, in the inverse mode. The fluid to solid density ratio is defined as $\delta = \rho_f/\rho_s$; time is scaled with $\pm(r_p/u_{zo})$; and β is scaled with $\pm(\rho_s u_{zo}/r_p)$. The particle phase pressure P_s and constant g_o are scaled with $\rho_s(u_{zo})^2$, and therefore always positive. Scaling results in two dimensionless groups: the Froude number (Fr) defined as $Fr = u_{zo}^2/g_z r_p$, and the particle Reynolds number defined as $Re_p = (\rho_s r_p \mid u_{zo} \mid)/\mu_s$. Re_p is computed at u_{zo}, and differs from Re computed at v_t, which is used to determine the Richardson-Zaki correlation index n (see equation 10). Re_p only considers fluid velocity *magnitude* $\mid u_{zo} \mid$ so that the sign of Re_p is always positive. This way, Reynolds number effects in the two bed modes can be compared without regard to flow direction. Using a factorization method [26], the velocity terms can be eliminated from equation 29 by substituting expressions for $\nabla \cdot \mathbf{u}\prime$ and $\nabla \cdot \mathbf{v}\prime$ from 26 and 27 into the divergence of equation 29 to obtain a single scalar equation, which is linear in the perturbation variable $\phi\prime$ [20]:

$$L\phi\prime = 0 \tag{30}$$

where the linear operator L is defined as

$$L = A\partial_{\bar{t}}^2 + 2\left(\tilde{C} - A\bar{\omega}\right)\partial_{\bar{t}}\partial_{\bar{z}} - M\Delta + \left(A\bar{\omega}^2 - 2\tilde{C}\bar{\omega} + \tilde{C}\right)\partial_{\bar{z}}^2$$

$$+E\partial_{\bar{t}} + (D - E\bar{\omega})\partial_{\bar{z}} + (J\bar{\omega} - H)\delta\partial_{\bar{t}} - J\delta\partial_{\bar{t}}$$

The overbar designates scaled variables, and Δ is the Laplacian operator. Substituting in the drag force coefficient β_o, evaluated under steady state conditions from equation 11, the coefficients in equation 30 are defined as

$$A = Fr\left[\frac{(1-\phi_o)}{\delta\phi_o} + 1 + \frac{C_o}{\phi_o(1-\phi_o)}\right]; \quad \tilde{C} = Fr\left(1 + \frac{C_o}{(1-\phi_o)}\right)$$

$$D = \frac{(1-\delta)\,n}{\delta}; \quad E = \frac{(1-\delta)}{\delta\phi_o}; \quad H = 0$$

$$J = \frac{Fr}{Re_p\phi_o}\frac{(1-\phi_o)}{\delta\phi_o}; \quad M = \frac{Fr\bar{P}\prime_{so}(1-\phi_o)}{\delta\phi_o}$$

When the base state of uniform fluidization is unstable, the fastest growing disturbance takes the form of a one-dimensional vertically traveling wave having no transverse structure. Thus, we seek a solution to equation 30 in the form of a plane wave disturbance $\phi\prime = \hat{\phi} exp(st) exp(\boldsymbol{\kappa} \cdot \boldsymbol{x})$ having a complex amplitude $\hat{\phi}$, and wavenumber vector $\boldsymbol{\kappa}$. The position vector is denoted by $\mathbf{x}$, and s represents a complex conjugate $s = \zeta \pm i\chi$. Substituting in the expression for $\phi\prime$ and its derivatives into 30, we obtain the following dispersion relation expressing wave velocity ω as a function of wavenumber $\boldsymbol{\kappa}$ (in one dimension) in the traveling wave frame:

$$A(s - i\kappa_z\omega)^2 + (s - i\kappa_z\omega)\left(E + 2i\tilde{C}\kappa_z + J\kappa_z^2\right) + iD\kappa_z + \left(M - \tilde{C}\right)\kappa_z^2 + iH\kappa_z^3 = 0 \tag{31}$$

The quantities s, ω and κ_z are scaled quantities unless specified otherwise. The overbars have been omitted for convenience. Eigenvalues $\sigma = s - i\kappa_z$ can thus be obtained from this dispersion relation in any traveling wave frame. In the laboratory frame ($\omega = 0$), complex eigenvalues $s_{1,2} = \zeta \pm i\chi$ describe one-dimensional periodic wave solutions satisfying the system of linearized equations 26 through 29 where the real part of s (ζ) determines the growth (or decay) rate of the disturbance, and the imaginary part (χ) determines the propagation velocity of the wave. In the laboratory frame of reference, it has been shown by Göz [25] and Göz *et al.* [1] that the base state is linearly stable to disturbances of small amplitude if the following two conditions are met:

$$f(d) \geq 0; \quad f(h) \geq 0$$

where $f(d)$ and $f(h)$ are *not* independent of one another, and

$$f(d) = m - c + 2cd - d^2, \;\; f(h) = m - c + 2ch - h^2 \tag{32}$$

$$m = M/A \quad , \quad c = \tilde{C}/A \quad , \quad d = D/E \quad , \quad h = H/J$$

This criterion is based upon the behavior of ζ, the real part of s at small and large wavenumbers. In each system this work examines, it can be shown that d is always greater than h and $f(h)$ is always greater than $f(d)$. Hence for all conditions $f(d) < 0$, the base state is unstable to small disturbances, and at $f(d) = 0$ the base state is marginally stable at some value ϕ_c. This condition allows us to calculate a minimum value for the particle pressure derivative $P\prime_{so}$ evaluated at $\phi_o = \phi_c$ at which point we might suspect the state of uniform fluidization loses stability. As recognized by Garg & Pritchett [11], the contribution of a force term in the momentum balance equations, proportional to the gradient of ϕ, and monotonically increasing with respect to ϕ, is necessary to stabilize the bed. The particle phase isotropic compressive force, P_s provides such a force term. It can be shown in this work that the stability of the uniform state is extremely sensitive to the Taylor series expansion of this term, and $P\prime_{so}$, is thus regarded as a valuable measure of bed stability in the neighborhood of the uniform base state. In this study we examined closures for P_s defined by equation 7. We see from the derivative of P_s that the value of the constant g_o is useful for comparing the stability of two fluidized systems at ϕ_c under identical operating conditions.

We know that a Hopf bifurcation point is possible when the vector field, which has been linearized about the base state, has a set of purely imaginary eigenvalues with all remaining eigenvalues having non-zero real parts. It is at these values that one-dimensional traveling waves bifurcate from the steady state solution. Göz & Sundaresan [20] show that by setting $s = 0$ in equation 31, we can obtain the propagation velocity of the wave ($\omega = \omega_{crit}$), and the critical wavelenth ($\kappa_z = \kappa_{crit}$) at the Hopf bifurcation point as,

$$\omega_{crit} = c + \left(c^2 + m - c\right)^{1/2} \qquad \kappa_{crit} = \left[\frac{E\left(d - \omega_{crit}\right)}{J\left(\omega_{crit} - h\right)}\right]^{(1/2)}$$

These results provide criteria for comparing the bifurcation structure of traveling wave solutions in the vicinity of ϕ_c.

4 Quasi-steady periodic solutions

In this section, we compute quasi-steady periodic solutions in the traveling wave frame (of reference). The derivation which follows is based upon that performed by Needham & Merkin [24] using two-phase continuum equations of continuity and motion describing a single-component gas-fluidized bed. The equations we derive consider the viscous and inertial effects of the fluid phase (including virtual mass), which were considered negligible by these authors in their analysis of gas systems. We consider one-dimensional vertical flow in normal and inverse fluidized beds for which equations 1 through 4 apply. We simplify matters by adding the two continuity equations 1 and 2 in the laboratory frame of reference ($\omega = 0$), and then integrate with respect to z to obtain the following equation in one-dimension z:

$$(1-\phi)u_z + \phi v_z = \tilde{M}(t) \tag{33}$$

where $\tilde{M}(t)$ is some function of time (constant with respect to space), and u_z and v_z are used to represent the locally averaged fluid and solid phase velocities respectively in the axial direction z. Equation 33 replaces equation 1 in this analysis. The non-dimensional equations can be written in one-dimension in the laboratory frame of reference as,

$$(1-\phi)\bar{u}_z + \phi\bar{v}_z = \bar{M}(t) \tag{34}$$

$$\frac{\partial\phi}{\partial\bar{t}} + \frac{\partial\left[\phi\bar{v}_z\right]}{\partial\bar{z}} = 0 \tag{35}$$

$$\phi\left[\frac{\partial\bar{v}_z}{\partial\bar{t}} + \bar{v}_z\frac{\partial\bar{v}_z}{\partial\bar{z}}\right] - \delta\phi\left[\frac{\partial\bar{u}_z}{\partial\bar{\mathrm{t}}} + \bar{u}_z\frac{\partial\bar{u}_z}{\partial\bar{\mathrm{z}}}\right] = \frac{4\eta}{3Re_p}\frac{\partial^2\bar{v}_z}{\partial\bar{z}^2} - \frac{\partial\bar{P}_s}{\partial\phi}\frac{\partial\phi}{\partial\bar{z}} - \frac{\phi}{Fr}(1-\delta) + \tag{36}$$

$$\frac{\phi(1-\delta)}{Fr}\frac{(1-\phi_o)^n}{(1-\phi)^n}(\bar{u}_z - \bar{v}_z) + \frac{\phi}{(1-\phi)}C\delta\left[\left(\frac{\partial\bar{u}_z}{\partial\bar{\mathrm{t}}} + \bar{u}_z\frac{\partial\bar{u}_z}{\partial\bar{\mathrm{z}}}\right) - \left(\frac{\partial\bar{v}_z}{\partial\bar{t}} + \bar{v}_z\frac{\partial\bar{v}_z}{\partial\bar{z}}\right)\right]$$

where all scaled quantities are represented with an overbar. The solid phase viscosity μ_s is scaled with the viscosity of the particle assembly at uniform fluidization condition, μ_{so}, evaluated at uniform solids volume fraction ϕ_o. This dimensionless quantity is defined as $\eta = \mu_s/\mu_{so}$. We assumed that the fluid and solid phase bulk viscosities λ and λ_s both equal zero, and the particle shear viscosity μ_s takes the form of expression 8. The drag coefficient β has been replaced by

$$\bar{\beta} = \frac{\phi(1-\delta)}{Fr}\frac{(1-\phi_o)^n}{(1-\phi)^n}$$

For simplicity, we assumed a linear form for P_s defined by equation 7 where $m_1 = 1$ and $m_2 = 0$ If the base state of uniform fluidization is unstable to small amplitude disturbances in voidage, a bifurcation to a family of traveling waves may be possible. We seek quasi-stationary periodic solutions to equations 34, 35 and 36 by transforming these equations to a frame of reference, which moves at the same velocity as the wave. We first introduce the moving coordinate system ($Y = z - \omega t$), where the wave velocity (ω) is a constant, and serves as the bifurcation parameter. We then transform the equations by incorporating the dimensionless derivatives $\partial_{\bar{z}} = \partial_{\bar{Y}}$ and $\partial_{\bar{t}} = -\bar{\omega}\partial_{\bar{Y}}$ where:

$$\begin{aligned} \omega &= \pm\bar{\omega}u_{zo} \\ \bar{Y} &= \bar{z} - \bar{\omega}\bar{t} \end{aligned}$$

At uniform fluidization, we know from equations 20 and 21 that $\bar{v}_z = 0$ and $\bar{u}_z = 1$. From equation 34, $\bar{M} = (1-\phi_o)$ and

$$\bar{u}_z = \frac{(1-\phi_o)}{(1-\phi_o)} - \frac{\phi}{(1-\phi_o)}\bar{v}_z \tag{37}$$

Transforming equation 35 to the traveling wave frame,

$$-\bar{\omega}\frac{\partial\phi}{\partial\bar{Y}} + \frac{\partial\left[\phi\bar{v}_z\right]}{\partial\bar{Y}} = 0 \tag{38}$$

and integrating with respect to $\bar{Y}$ yields $\phi\left(\bar{v}_z - \bar{\omega}\right) = \bar{N}$ where $\bar{N}$ is a constant. Using conditions at uniform fluidization, we find $\bar{N} = -\phi_o\bar{\omega}$, and

$$\bar{v}_z = \bar{\omega}\left(1 - \frac{\phi_o}{\phi}\right) \tag{39}$$

Substituting the expressions for $\bar{u}_z$ and $\bar{v}_z$ (from 37, 39) and their derivatives with respect to $\bar{Y}$ into equation 36 yields a single second order equation in ϕ. Since we seek periodic solutions to equation 36, we work in the phase plane (ϕ, Ω), where $\Omega = d\phi/d\bar{Y}$, and write two first order differential equations,

$$f_1 = \frac{d\phi}{d\bar{Y}} = \Omega \tag{40}$$

$$\begin{aligned} f_2 = \frac{d\Omega}{d\bar{Y}} = \frac{2\Omega^2}{\phi} + B\phi^2\left[\bar{g}_o - \frac{\phi(1-\phi_o)^2(1-\bar{\omega})^2\delta}{(1-\phi)^3}\left(1 + \frac{C}{(1-\phi)}\right) - (\frac{\bar{\omega}\phi_o}{\phi})^2\left(1 + \frac{C\delta}{(1-\phi)}\right)\right]\Omega \\ - \frac{B\phi^3(1-\delta)}{Fr(1-\phi)^{(n+1)}}\left[(1-\phi_o)^{(n+1)}(1-\bar{\omega}) - (1-\phi)^{(n+1)} + \frac{\bar{\omega}\phi_o}{\phi}(1-\phi_o)^n(1-\phi)\right] \end{aligned} \tag{41}$$

where the coefficient B is defined as,

$$B = \left(\frac{3Re_p}{4\eta\bar{\omega}\phi_o}\right)$$

The simplest solution to equations 40 and 41 is that which represents the uniform fluidized state, $\phi = \phi_o$ and $\Omega = 0$. Periodic solutions corresponding to traveling waves are closed orbits, which surround the equilibrium state $(\phi_o, 0)$ in the phase plane (ϕ, Ω). Such solutions are found by determining the two eigenvalues $s_{1,2} = \zeta \pm i\chi$ of the linearized equations f_1 and f_2, which are

$$s_{1,2} = \frac{1}{2}\left[tr\tilde{\mathbf{J}} \pm \sqrt{(tr\tilde{\mathbf{J}})^2 - 4 \mid \tilde{\mathbf{J}} \mid}\right]$$

where $\tilde{\mathbf{J}}$ is the Jacobian matrix.

5 Results

5.1 Linear stability analysis

In this section, we examine instabilities of fluidized beds operating in *normal* and *inverse* mode. The beds have been uniformly expanded with water to reach a marginally stable and spatially uniform steady state defined by a critical solids volume fraction $\phi_c = \phi_o$. We investigated the stability of this base state against perturbations to the flow distribution in the form of localized voidage disturbances of small amplitude. In order to investigate the effect of the Fr number on overall bed stability, we considered examples of normal and inverse beds having comparable Fr numbers and Fr numbers, which differed by as much as a 4:1 ratio. We focused on this dimensionless group because of its identified importance in distinguishing instability behavior in gas- and liquid-fluidized beds as reported in the theoretical and experimental literature.

In the experimental work of Wilhelm & Kwauk [7], bed behavior is differentiated as being either *particulate* (having greater operational stability), or *aggregative* (exhibiting more complex bubbling behavior) based primarily on the Fr number. These authors predict that the higher the

Fr, the more likely the bed is to *bubble*, and exhibit aggregative behavior. Attempts to confirm the empirical significance of the Fr number have successfully been made by other researchers. For example, Anderson *et al.* [14] and Glasser *et al.* [22] show qualitative differences in the structure of two-dimensional traveling wave forms, which bifurcate from the uniform fluidization state in a two-dimensional stability analysis of gas- and liquid-fluidized beds. Gőz & Sundaresan [20] show similar results in a low amplitude analysis. However, Fr numbers in gas- and liquid-fluidized systems can vary by several orders of magnitude. The inverse mode of operation provides a unique opportunity to take a closer look at the effect of fluidization direction and Fr number in uniformly fluidized beds described by two sets of subtly varying dimensionless groups.

Case I: Comparable Fr number

At this stage, it is useful to consider some specific examples of water-fluidized beds whose particle properties are shown in Table 1. We have chosen two systems, *Case* **I** and *Case* **II**, which are realistic so that future experimental work might be possible. We first consider the example of *Case* **I**; the bed operating in normal mode consists of $775\mu m$ water saturated carbon char particles ($\rho_s = 1500\ kg/m^3$), and the inverse bed consists of $1000\mu m$ plastic particles ($\rho_s = 666.7\ kg/m^3$). The particles are considered to be spherical, and the wall-effects of the fluidization column are not considered in the calculation of rising and settling velocities. Particle size and density were selected, such that the terminal settling velocity in normal mode would be exactly equivalent to the terminal rising velocity in inverse mode for an individual particle in an infinite volume of fluid. As a result, the Fr numbers are comparable in magnitude and always positive because of the squared u_{zo} term; however, they are not identical. The diameter of the low density plastic particles is 25% larger than the carbon in order to obtain equivalent rising and settling velocities. We have not specified the plastic material, only its density and size. However, we have assumed that the plastic has a non-porous surface, although it may be impregnated with air. As a basis for comparison,

Table 1: Particle properties of water fluidized beds: Case I & II

Particle Properties					
Case	*Bed Type*	*Material*	d_p (μm)	ρ_s (kg/m^3)	$\dagger v_t$ (mm/s)
I	normal	carbon-char*	775	1500**	50.4
	inverse	plastic	1000	666.7	-50.4
II	normal	glass beads	1000	2200	126.0
	inverse	plastic	1000	454.5	-71.7

* water impregnated

**mean density of water saturated hollow char

† velocity in the intermediate flow regime calculated using Denn (1980).

we chose to look at bed conditions at a critical solids volume fraction of $\phi_c = 0.576$ [23]. The dimensionless parameters for *Case* **I** under these conditions are shown in Table 2 for the two modes of operation. The minimum particle pressure constant $g_o(min)$ was computed at the point when the bed is marginally stable at ϕ_c using the non-linear closure for P_s taken from equation 7 with $m_1 = 1$ and $m_2 = 2$, and the stability condition from [20] (see equation 32). The normal bed has a fluid to solid density ratio δ_{norm}, which is reciprocal to that of the inverse bed $\delta_{inv} = 1/\delta_{norm}$. All dimensionless quantities are based on a length scale of r_p and velocity scale $\pm(u_{zo})$. Based on linear

Table 2: Dimensionless parameters of water fluidized beds at $\phi_c = 0.576$: Case I & II

Dimensionless Bed Parameters						
Case	Bed Type	δ_{norm} δ_{inv}	Re_p $\times 10^3$	Fr $\times 10^2$	$g_o(min)$ $\times 10^3$	$\dagger u_{zo}$ mm/s
I	normal	1/1.5	6.7	1.9	2.3	8.4
	inverse	1.5/1	4.1	1.7	3.5	-9.0
II	normal	1/2.2	42.6	16.2	1.4	28.2
	inverse	2.2/1	6.4	4.0	4.3	-14.0

† fluidization velocity at ϕ_c =0.576 in water.

stability results of primary instabilities in gas- and liquid-fluidized beds [20], one might expect that the limiting value of $g_o(min)$ would be greater in the bed having the higher Fr number (in this case, the normal bed). This reasoning is consistent with the criterion established by Wilhelm & Kwauk [7]. In *Case* **I** however, $g_o(min)$ is greater in the inverse bed of plastic particles even though the Fr number is slighly lower than in the normal bed of carbon particles. In fact, it can be shown from equation 32 that at the point of marginal stability ($f_d = 0$ at $\phi_o = \phi_c$), the constant $g_o(min)$ is independent of Fr and a function only of the fluid to particle density ratio δ. We now move on to investigate the effect of Fr number on relative instability strength, which we have measured using both the magnitude of the maximum dimensionless growth rate $\mid \zeta_{max} \mid$ and the critical wavenumber κ_{crit} at which saturated one-dimensional traveling waves bifurcate from the steady state solution.

The linear stability of the uniform state against one-dimensional disturbances is illustrated in figures 1(a) and 1(b) for the *Case* **I** normal and inverse beds, respectively, whose properties and dimensionless parameters are described in Tables 1 and 2. In these figures, the real part (ζ) of the complex growth rate (s) of a one-dimensional, vertically traveling disturbance is plotted versus the wavenumber κ_z for a range of ϕ_o ($\leq \phi_c$) values. The plotted quantities are dimensionless, and since the units for ζ are reciprocal seconds (s^{-1}), the growth rate is scaled with $-(u_{zo}/r_p)$ in the inverse bed. We have thus plotted $-\zeta$ versus κ_z in figure 1(b) so that actual growth (or decay) of the wave is obvious to the reader. We have examined the linear stability of the base state for various ϕ_o values, which are indicated in the figure captions. Computed results for the *Case* **I** stability analysis are tabulated in Table 3 for direct comparison. Figures 1(a) and 1(b) show that both beds are stable at all vertical wavenumbers for $\phi_o \geq \phi_c$ since the (dimensional) real part of s is always less than zero in this range. At $\phi_c = 0.576$, the bed is considered to be marginally stable. For $\phi_o < \phi_c$, the uniform state is unstable for a finite range of κ_z values. As ϕ_o decreases, the bed becomes more unstable at higher values of κ_z, and there is a corresponding increase in the maximum (dimensionless) growth rate of the wave (indicated by $\mid \zeta_{max} \mid$) as shown in Table 3. In this table, we have also included the dimensional maximum growth rate ζ^*_{max} to compare the relative magnitudes of the growth rates in

Table 3: Linear stability of water fluidized beds at values $\phi_o < \phi_c$: Case I & II

Case	Bed Type	ϕ_o	Fr $\times 10^2$	g_o $\times 10^3$	$\mid \zeta_{max} \mid$ $\times 10^4$	ζ^*_{max} $\times 10^3$	$\dagger\omega_{crit}$	$\dagger\kappa_{crit}$
I	norm	0.57	2.0	2.1	2.0	4.5	1.58	0.138
	inv		1.7	3.3	1.5	2.8	1.55	0.134
	norm	0.55	2.4	1.8	17.0	41.8	1.10	0.318
	inv		2.1	2.8	14.5	29.4	1.11	0.308
	norm	0.54	2.6	1.6	25.0	64.4	0.91	0.400
	inv		2.3	2.5	21.5	45.6	0.93	0.390
II	norm	0.57	17.1	1.3	5.0	28.9	1.40	0.153
	inv		4.2	4.1	2.0	5.8	1.51	0.135
	norm	0.55	20.0	1.1	65.0	407.0	0.96	0.361
	inv		5.0	3.4	17.0	53.4	1.09	0.310
	norm	0.54	21.6	1.1	100.0	651.0	0.78	0.463
	inv		5.5	3.1	26.0	85.2	0.90	0.396

Linear Stability Analysis

$*$ *dimensional* maximum growth rate evaluated at ϕ_o having units of s^{-1}.

$\dagger$ evaluated at the Hopf bifurcation point

the two beds.

We can see from these figures and from the tabulated data that both ζ^*_{max} and $\mid \zeta_{max} \mid$ corresponding to the higher Fr (in this case, the normal bed of carbon) are always greater than those for the lower Fr (inverse bed). These data suggest that instabilities occurring in the neighborhood of the base state in normal fluidization grow at a much faster rate than in the inverse bed, even though the inverse bed has a higher propensity to become unstable as previously recognized. We have thus considered two measures of bed stability; *viz.* the *propensity* of the bed to become unstable, as measured by the relative value of $g_o(min)$ computed at ϕ_c; and the *strength* of the instability, as measured by the maximum growth rates ζ^*_{max} and $\mid \zeta_{max} \mid$ of traveling wave solutions. These results are consistent with the results of [20] for gas and liquid systems when one considers their dimensional predictions of maximum growth rate. These authors found that dimensional growth rates in the air-fluidized system, having a Fr four orders of magnitude greater than the water-fluidized system, were considerably larger than the water-fluidized bed, which we know to be less unstable than the air-fluidized bed.

In figures 1(a) and 1(b), let us choose the curve representing $\phi_o = 0.54$. Beginning at the far right hand side of the x axis, or highest value of κ_z, and moving to the left, we encounter a critical wavenumber value κ_{crit} at point **A** where $\zeta = 0$, and the two eigenvalues become purely imaginary. This point is a Hopf bifurcation point, and signals the birth of a family of one-dimensional traveling wave solutions. Each traveling wave solution moves at a dimensionless wave velocity ω relative to the laboratory frame of reference, which can be determined as part of the solution. If one were to travel in a moving frame of reference at velocity ω, the solution would appear to be a steady state. The Hopf bifurcation points for the values of $\phi_o = 0.54$ and $\phi_o = 0.57$ are labeled **A** and **B** respectively, and the values of κ_{crit} and ω_{crit} are tabulated in Table 3 for these points and at other ϕ_o conditions. Note that the κ_{crit} values are consistently higher in the normal bed, especially at the lower ϕ_o values, and that these results are consistent with higher reported values of $\mid \zeta_{max} \mid$. The effect of Fr number and the fluid to solid density ratio δ on instability strength are further examined in *Case* **II** to follow where beds are selected having Fr numbers differing by a factor of 4 to 1 respectively.

Case II: Fr number differing by 4:1

We attempted to add to our understanding by considering another case (*Case* **II**) of water-fluidized normal and inverse beds having δ_{norm} and δ_{inv}, which are further from unity than in the *Case* **I** systems. In this case, 1000 μm heavy glass beads ($\rho_s = 2200\ kg/m^3$) and 1000 μm light plastic particles ($\rho_s = 454.5\ kg/m^3$) are fluidized with water under Fr number conditions differing by a factor of 4 to 1 respectively. The large particle density difference of the glass and plastic contributes significantly to the variation in Fr because of the difference in terminal rising and settling velocities of the equi-sized particles. Particle properties for the *Case* **II** systems are shown in Table 1; the dimensionless parameters are shown in Table 2 at equilibrium conditions $\phi_c = 0.576$. In an experimental system, these fluidized beds would *visually* appear identical if the particles were the same color and the beds were both uniformly stable at constant bed voidage. Note in Table 2 that the computed value for $g_o(min)$ in the inverse plastic bed is three times that for the normal glass bed despite the four fold Fr number difference. Based upon the imposed stability criteria, these results confirm previous findings that the propensity of the bed to destabilize is a function of δ and independent of u_{zo}^2 ($1/r_p$ is the same in this case). The uniformly fluidized inverse bed thus appears to be less stable to perturbations than the normal bed at ϕ_o values close to ϕ_c due to the ratio of fluid to solid density alone.

The results of a linear stability analysis of the uniformly fluidized systems in *Case* **II** are reported in Table 3 for various values of ϕ_o close to ϕ_c. We can see from these data that the growth rates of the disturbances also follow the same trend as observed in *Case* **I**, i.e., $\mid \zeta_{max} \mid$ and ζ^*_{max} are much greater in the glass system having the higher Fr number. However, the variation in growth rate is more dramatic in the glass & plastic beds suggesting a strong dependency on the square of the fluid velocity term. Moreover in *Case* **II**, we see in Table 3 that the Hopf bifurcation points of the uniform base state in the glass bed occur at higher wavenumber values κ_{crit}, and corresponding lower ω_{crit} values than in the plastic bed for every ϕ_o value we examined. This means that when the normal bed becomes unstable, one-dimensional traveling waves in the glass bed grow at a faster rate and propagate through the bed at a slower velocity than waves moving through the inverse bed. These results are consistent with growth rate predictions suggesting the relative strength of unstable waveforms within the δ range investigated can be predicted based primarily on Fr number with some dependency on δ as shown in *Case* **I**. This conclusion is consistent with ideas put forth previously.

In summary, the Fr number appears to be an important parameter with respect to predicting instability strength, but has no effect on the propensity of the bed to destabilize, since we have shown that the inverse bed is significantly less stable to perturbations regardless of Fr in all the case studies examined. These results suggest that δ controls the onset of an instability, and that the strength of the instability is strongly influenced by Fr and to a lesser extent, δ. The experimental and theoretical literature clearly show a correlation between Fr number and the likelihood of gas- and liquid-fluidized systems to exhibit bubbling behavior when the inertial and viscous effects of the gas system are neglected. It is important to point out that Fr number variation in gas- and liquid-fluidized systems is quite significant (varying by orders of magnitude) compared to the subtle variations observed in the water-fluidized systems examined here. Moreover, liquid fluidized beds are far less likely to "bubble".

So far, we have examined the linear stability of the uniform base state using the bed voidage ϕ_o as the basis for comparison. This seemed reasonable, since the particle pressure term plays a dominant role in bed stabilization, and we have represented it as an increasing function of solids volume fraction. We now move to the traveling wave frame to compute one-dimensional traveling wave solutions (1D-TW's) emanating from Hopf bifurcations of the steady state solution. We compare the bifurcation diagrams and high amplitude wave profiles of 1D-TW's, which can *suggest* the structure of fully developed wave forms.

5.2 One-dimensional traveling waves

Periodic solutions describing a family of one-dimensional traveling waves were computed numerically using a continuation technique from the software package AUTO (Doedel [31]). This software was used to compute branches of periodic solutions satisfying the ordinary differential equations 40 and 41 in the phase plane (ϕ, Ω). We made use of a continuation scheme, which starts at a Hopf bifurcation of the uniform fluidization state, and uses ω as the continuation or bifurcation parameter. We present results for the glass bead and plastic beds constituting the *Case* **II** systems, which were previously discussed and whose particle properties and dimensionless parameters are shown in Tables 1 and 2 respectively. The developed wave structures and amplitudes are much more dramatic in this case than in the carbon and plastic *Case* **I** analysis. The results for the carbon and plastic beds are qualitatively similar however, and the same conclusions were arrived at in both cases regarding the behavior of one-dimensional traveling wave structures in inverse and normal beds.

Figure 2(a) is a bifurcation diagram of one-dimensional periodic wave solutions, which were numerically computed for the normal bed of water-fluidized glass beads. In this figure, the l_2-norm of Ω, $|| \Omega ||$ is plotted as a function of (dimensionless) wavespeed ω, where $|| \Omega ||$ gives a measure of the amplitude of the solution with respect to the uniform state. A Hopf bifurcation of the steady state solution $(\phi_o = 0.54, \Omega = 0)$ is represented by point **A** in this figure, and is the starting point of the continuation scheme. We see that $|| \Omega ||$ *increases* with increasing ω, eventually reaching a maximum point at $\omega \approx 1$ corresponding to point **Q**. Beyond this point, $|| \Omega ||$ decreases steadily with increased wavespeed. Here, waves become steeper and have greater amplitude as the fluctuation of volume fraction increases about ϕ_o. In numerical simulations of bubbling behavior in normal mode gas-fluidized beds, Anderson *et al.* [14] show that high amplitude, two-dimensional traveling wave solutions have bubble-like holes with fluid traveling upwards through the center of the hole. Particles accelerate downwards through the 'roof' (or top) of the bubble, but then begin to decelerate as they move downwards though the bubble, and exit through the bubble 'floor'. The structure developed by this velocity field exhibits a high voidage fluid floor with a rounded roof of higher particle concentration. These authors show that the asymmetry exhibited in one-dimensional solutions at high amplitude is indicative of this structure formation.

Periodic solutions describing high amplitude traveling waves, having increased steepness and a more defined structure, were numerically computed at increased wavespeeds for the system of glass beads in water. For very steep waves, the computational scheme failed, and further continuation could not be carried out. Traveling wave profiles computed in the vicinity of point **S** on the bifurcation diagram figure 2(a) are shown in figure 3(a) where (dimensionless) $Y = z - \omega t$ is plotted versus ϕ. In this figure, the asymmetry of the wave structure becomes apparent. Notice that, as one moves up the y axis from the origin, ϕ transitions abruptly in the area labelled **[1]**, and decreases rapidly to a minimum ϕ value. Volume fraction then transitions back to baseline in a more gradual manner in the area labelled **[2]**. The asymmetry exhibited by the one-dimensional structure is described by a sharp flattened 'floor' represented by transition **[1]**, and rounded 'roof' represented by transition **[2]**, where 'top' and 'bottom' are defined with respect to the positive vertical axis $+z$.

The bifurcation diagram for the complementary inverse bed of plastic particles in water is shown in figure 2(b). Although the bifurcation structure is similar in both bed modes, the bifurcation occurs at a higher ω_{crit} value (labelled point **A**) in the inverse bed, and waves have slightly lower amplitudes. This is because instabilities were found to be weaker in the inverse bed, as measured by comparatively higher ω_{crit} and lower κ_{crit} values. Based on the bifurcation diagrams alone, instability behavior in the two bed modes cannot be distinquished on a qualitative basis. However, high amplitude wave solutions computed in the vicinity of point **R** in figure 2(b) are illustrated in figure 3(b), and describe structures, which are distinct from those computed in the normal bed of glass beads (curve **S**, figure 3(a)). In particular, high amplitude one-dimensional wave profiles in the inverse bed develop very steep, *shock-like* fronts as one moves *down* the y axis. Abruptly, there is a step change in volume fraction ϕ located at point **[1]** in figure 3(b). With an incremental decrease in Y, the system returns to constant ϕ in a more gradual way (area labelled **[2]**). The asymmetry suggests a bubble 'floor' at point **[1]** and bubble 'roof' located below it with respect to the vertical axis $+z$. The one-dimensional wave structure would appear to be "flipped" over relative to a wave in the normal bed propagating upwards in the column in the $+z$ direction. Results also show that 1D-TW's in the inverse bed always propagate in the direction of gravity for all the case studies examined.

In summary, we have shown that high amplitude one-dimensional traveling wave solutions computed from Hopf bifurcation points using a continuation scheme in the bifurcation parameter ω become steep and highly asymmetric, and that high amplitude 1D-TW's become shock-like in the inverse beds we examined. Moreover, the asymmetry of 1D-TW's of high amplitude is *reversed* about the vertical axis suggesting that fully developed bubble-like structures (indicated by asymmetrical one-dimensional solutions) are *flipped* over in the two bed modes. This suggests that the orientation of a (fluid filled) bubble 'floor' and (particle filled) bubble 'roof' are reversed with respect to the axial dimension z and that the direction of wave propagation in the two bed modes is consistent with these findings.

6 Conclusions

The inverse fluidized bed has provided an opportunity to examine unstable flow behavior in beds, which are described by a range of dimensionless groups not physically realized in normal fluidization mode. In a linear stability analysis of various sets of uniformly fluidized normal & inverse beds, the dimensionless Fr number and (to a lesser extent) fluid to solid density ratio δ were shown to be indicators of instability *strength*, based upon bifurcation structure and growth rates of one-dimensional traveling wave solutions. The effect of Fr and δ on instability strength was confirmed in three case studies of water-fluidized normal & inverse beds having reciprocal fluid to solid density ratios and operating under identical, similar and differing Fr number conditions. These results are consistent with experimental and theoretical evidence showing a correlation between Fr number and the likelihood of gas- and liquid-fluidized systems to exhibit bubbling behavior. The fluid to solid density ratio δ was shown to be significant with respect to instability *onset*, defined by the conditions under which the uniformly fluidized bed is rendered marginally stable. In particular, it has been shown that, at the point of marginal stability, the particle pressure constant $g_o(min)$ is independent of Fr and a function only of the fluid to particle density ratio δ.

In all of the case studies examined, the computed traveling wavespeed ω was shown to be in the *direction* of fluid flow. We know from the experimental literature that voidage waves travel upwards through the bed in normal mode fluidization, but since there is no experimental evidence of inverse bed behavior, we can only presume that disturbances propagate downwards through the bed, and perturbations in the positive vertical direction (against fluid flow) are damped out. Moreover, high amplitude, one-dimensional traveling wave solutions were steep and highly asymmetrical about the horizontal axis where the asymmetry was *reversed* or “flipped over” in the two bed modes. This suggests that fully developed bubble-like structures are orientated in the direction of fluid flow with respect to a particle rich bubble ‘roof’ and fluid-filled bubble ‘floor’. Results from these analyses naturally suggest a comprehensive experimental study be carried out to bring forth further qualitative differences in the unstable flow regime.

In a case study involving normal and inverse beds operating under equivalent Fr number conditions, results show eigenvalue structure to be identical in the two modes, and therefore independent of the quantity δ. Although the bifurcation structure of the steady state solution is qualitatively similar in the two bed modes, Hopf bifurcation points differ quantitatively in a way that is consistent with linear stability results of beds with differing Fr numbers. This confirms that δ along with Fr number affects the strength of one-dimensional waves as measured by the critical wavenumber at the Hopf bifurcation.

7 References

[1] Gőz, M.F., Glasser, B.J., Kevrekidis, Y.G., Sundaresan, S. (1996), Traveling waves in multi-phase flows, In M. Rahman (Ed.), *Advances in Fluid Mechanics*, Vol. 9 (pp 307-316). Boston: Computational Mechanics Publications.

[2] Muroyama, K. & Fan, L. S. (1985). Fundamentals of gas-liquid-solid fluidization, *A.I.Ch.E. Journal*, *31(1)*, 1-34.

[3] Fan, L.S., Muroyama, K., Chern, S.H., (1982), Hydrodynamic characteristics of inverse fluidization in liquid-solid and gas-liquid-solid systems, *Chemical Engineering Journal* **24**, 143-150.

[4] Krishnaiah, K., Guru, S., Sekar, V., (1993), Hydrodynamic studies on inverse gas liquid solid fluidization, *Chemical Engineering Journal* **51**, 109-112.

[5] Comte, M.P., Bastoul, D., Hebrard, G., Roustan, M., Lazarova, V., (1997), Hydrodynamics of a three-phase fluidized bed - the inverse turbulent bed, *Chemical Engineering Science* **52**, 3971-3977.

[6] Gibilaro, L.G., (2001), *Fluidization-dynamics.* Oxford: Butterworth-Heinemann.

[7] Wilhelm, R. H. & Kwauk, M. (1948). Fluidization of solid particles. *Chemical Engineering Progress*, *44*, 201-218.

[8] Pigford, R. L. & Baron, T. (1965). Hydrodynamic stability of a fluidized bed. *Industrial and Chemistry Engineering Fundamentals*, *4*, 81-87.

[9] Murray, J.D., (1965), On the mathematics of fluidization. Part I: Fundamental equations and wave propagation, *J. Fluid Mech.* **21**, 465-493.

[10] Anderson, T.B., Jackson, R., (1967), A fluid mechanical description of fluidized beds: equations of motion, *Ind. Eng. Chem. Fund.* **6**, 527-534.
[11] Garg, S.K., Pritchett, J.W., (1975), Dynamics of gas-fluidized beds, *J. Appl. Phys.* **46**, 4493-4500.
[12] Batchelor, G.K., (1988), A new theory of the instability of a uniform fluidized bed, *J. Fluid Mech.* **193**, 75-110.
[13] Koch, D.L., Sangani, A.S., (1999), Particle pressure and marginal stability limits for a homogeneous monodisperse gas-fluidized bed: kinetic theory and numerical simulations, *J. Fluid Mech.* **400**, 229-263.
[14] Anderson, K., Sundaresan, S. and Jackson, R. (1995), Instabilities and the formation of bubbles in fluidized beds, *J. Fluid Mech.* **303**, 327-366.
[15] Duru, P., Nicolas, M., Hinch, E.J., Guazzelli, È., (2002), Constitutive laws in liquid-fluidized beds, *J. Fluid Mech.* **452**, 371-404.
[16] Duru, P., Guazzelli, È., (2002), Experimental investigation on the secondary instability of liquid-fluidized beds and the formation of bubbles, *J. Fluid Mech.* **470**, 359-382.
[17] Gőz, M.F., (1993a), Bifurcation of plane voidage waves in fluidized beds, *Physica D* **65**, 319-351.
[18] Gőz, M.F., (1993b), Instabilities and the formation of wave patterns in fluidized beds. In *Instabilities in Multiphase Flows*, G. Gouesbet and A. Berlemont, Ed., Plenum, 251-259.
[19] Gőz, M.F., (1995a), Small Froude number asymptotics in two-dimensional two-phase flows, *Phys. Rev. E.* **52**, 3697-3710.
[20] Gőz, M.F., Sundaresan, S., (1998), The growth, saturation, and scaling behaviour of one- and two-dimensional disturbances in fluidized beds, *J. Fluid Mech.* **362**, 83-119.
[21] Gőz, M.F., (1995b), Transverse instability of plane wavetrains in gas-fluidized beds, *J. Fluid Mech.* **303**, 55-81.
[22] Glasser, B.J., Kevrekidis, I.G., Sundaresan, S., (1996), One- and two-dimensional travelling wave solutions in gas-fluidized beds, *J. Fluid Mech.* **306**, 183-221.
[23] Glasser, B.J., Kevrekidis, I.G., Sundaresan, S., (1997), Fully developed travelling wave solutions and bubble formation in fluidized beds, *J. Fluid Mech.* **334**, 157-188.
[24] Needham, D. J. & Merkin, J. H. (1986). The existence and stability of quasi-steady periodic voidage waves in a fluidized bed. *Journal of Applied Mathematics and Physics (ZAMP)*, *37*, 322-339.
[25] Gőz, M.F., (1992), On the origin of wave patterns in fluidized beds, *J. Fluid Mech.* **240**, 379-404.
[26] Anderson, T.B., Jackson, R., (1968), A fluid mechanical description of fluidized beds: stability of the state of uniform fluidization, *Ind. Eng. Chem. Fund.* **7**, 12.
[27] Johnson, P.C., Jackson, R., (1987), Frictional-collisional constitutive relations for granular materials, with application to plane shearing, *J. Fluid Mech.* **176**, 67-93.
[28] Richardson, J. F. & Zaki, W. N. (1954). Sedimentation and fluidisation: Part I. *Transactions of the Institute of Chemical Engineers*, *32*, 35-53.
[29] Denn, M.M., (1980), *Process Fluid Mechanics.* Englewood Cliffs, NJ: Prentice Hall.
[30] Berryman, J.G., (1982), Random close-packing of hard spheres and disks, *Phys. Rev.* A**27**, 1053-1062.
[31] Doedel, E., (1986), AUTO: Software for continuation and bifurcation problems in ordinary differential equations.
[32] Needham, D. J. & Merkin, J. H. (1983). The propagation of a voidage disturbance in a uniformly fluidized bed. *Journal of Fluid Mechanics*, *131*, 427-454.
[33] Richardson, J. F. (1971). In: J. F. Davidson and D. Harrison (Ed.), *Fluidization.* New York: Academic Press.

Figure 1

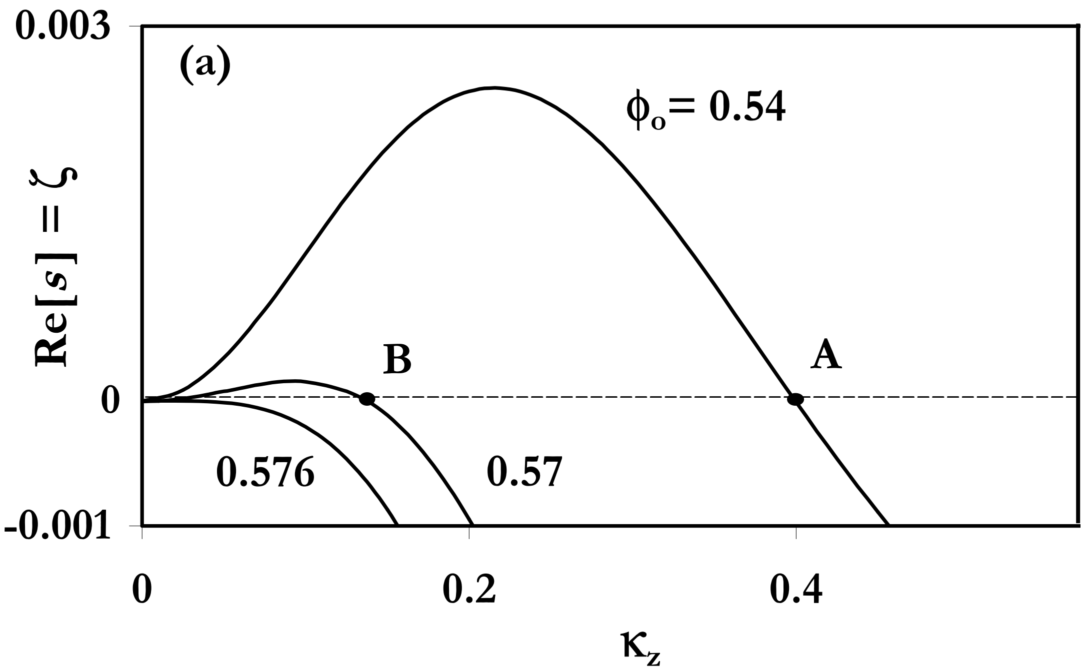

Figure 1

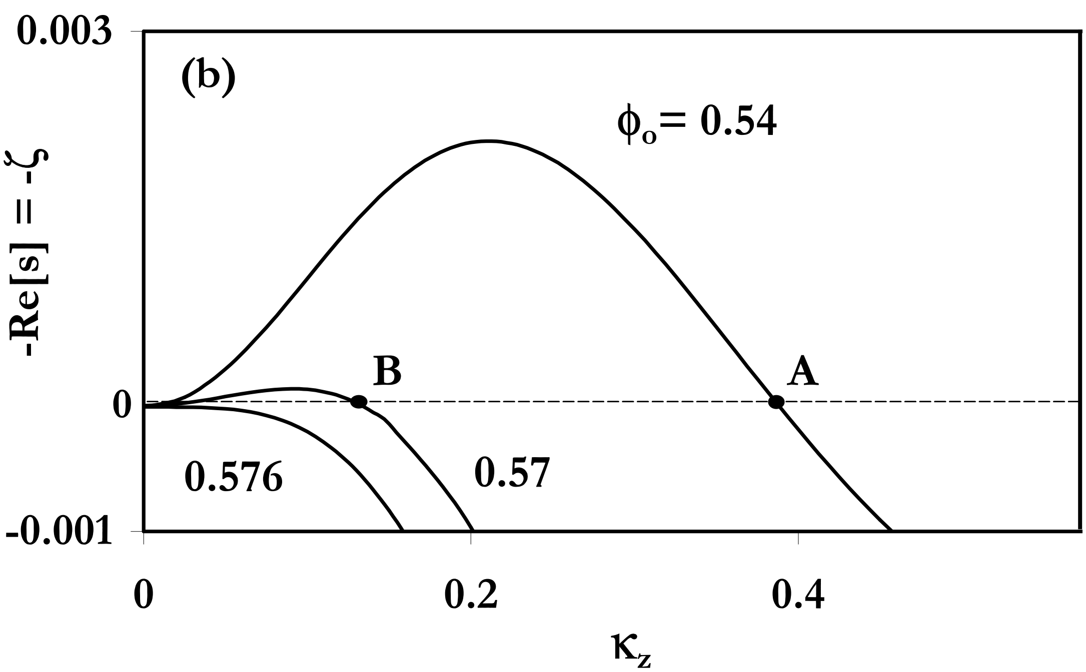

Figure 1: Case I: Linear stability of the uniform state. Real part of the (complex) growth rate ($s=\zeta+i\chi$) as a function of κ_z for various values of $\phi_o \leq \phi_c = 0.576$. Hopf bifurcation points located at **A** and **B**. All quantities are dimensionless.

(a) Normal bed of 775 μm carbon particles in water. Points **A** ($\kappa_{crit} = 0.400$, $\phi_o = 0.54$) and **B** ($\kappa_{crit} = 0.138$, $\phi_o = 0.57$).
(b) Inverse bed of 1000 μm plastic particles in water. Points **A** ($\kappa_{crit} = 0.389$, $\phi_o = 0.54$) and **B** ($\kappa_{crit} = 0.134$, $\phi_o = 0.57$).

Figure 2

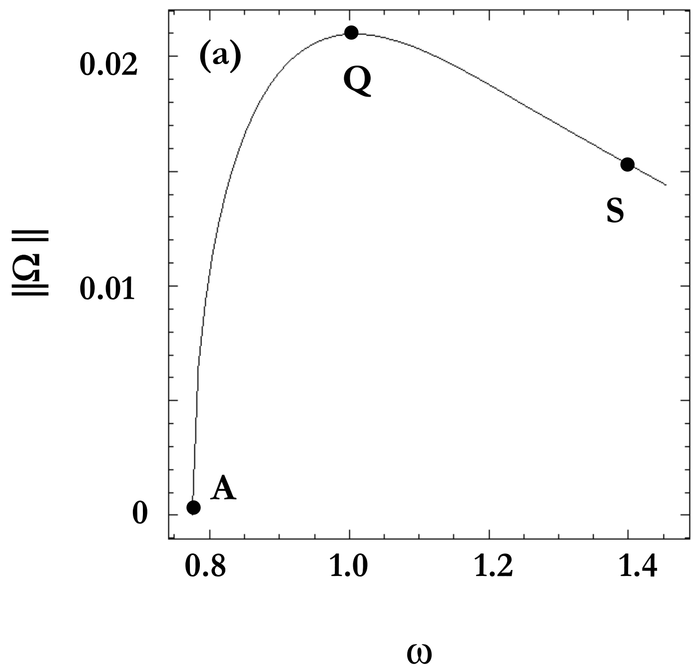

Figure 2

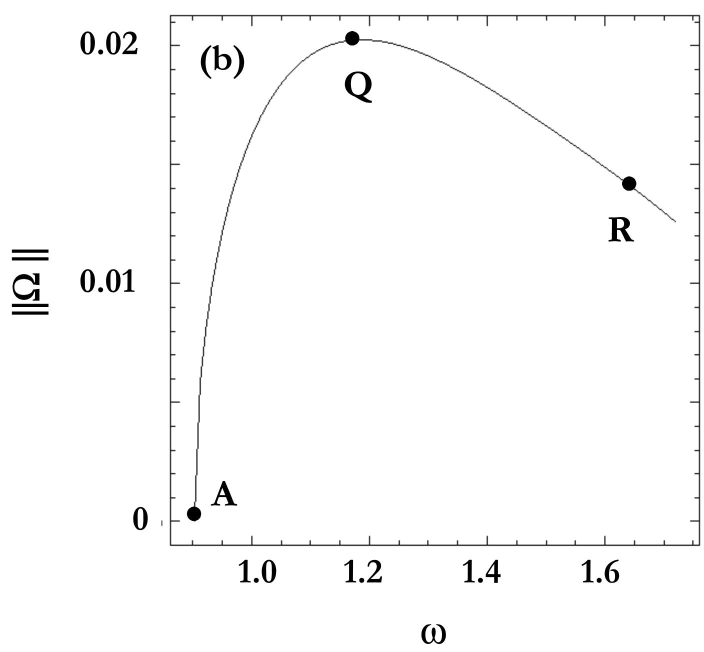

Figure 2: Case II: Bifurcation diagram for one-dimensional traveling waves. The l_2 norm $\|\Omega\|$ versus bifurcation parameter ω in water fluidized beds. Hopf bifurcation (point **A**) at equilibrium point (0.54,0). Point **Q** corresponding to $\|\Omega\|_{max}$. Continuation scheme fails in the vicinity of points **S** and **R**. All quantities are dimensionless.

(a) Normal bed of 1000 μm glass beads in water. Point **A** at ω_{crit} = 0.76, κ_{crit} = 0.463.
(b) Inverse bed of 1000 μm plastic particles in water. Point **A** at ω_{crit} = 0.90, κ_{crit} = 0.396.

Figure 3

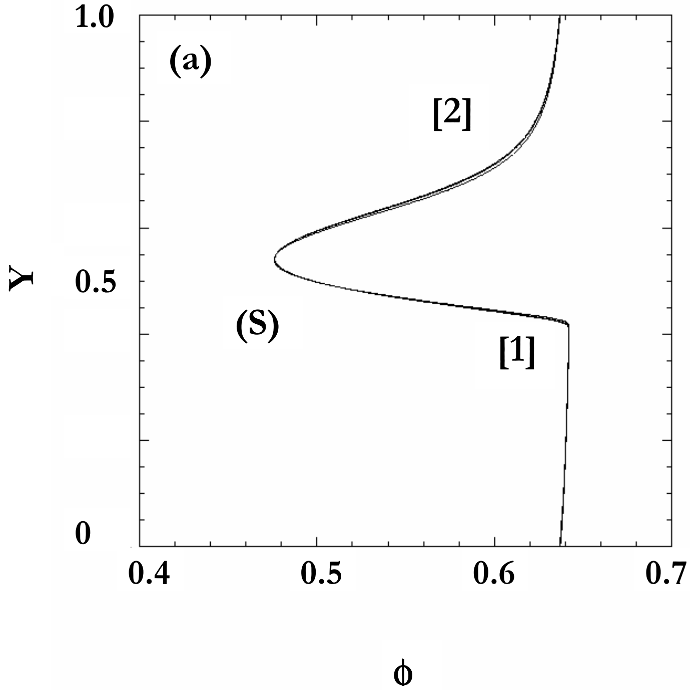

Figure 3

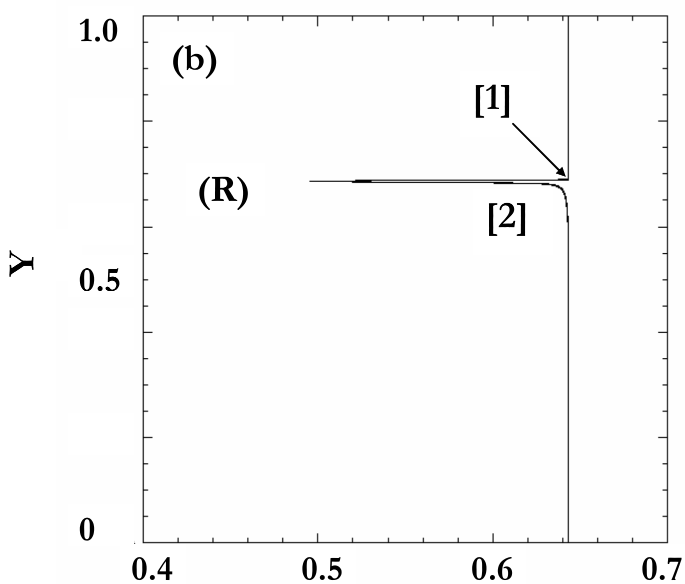

Figure 3: Case II: Asymmetrical traveling wave profiles corresponding to high amplitude one-dimensional traveling wave solutions computed in the vicinity of points **S** and **R** in figures 2(a) and 2(b) respectively. (Dimensionless) $Y=z-\omega t$ versus solids volume fraction ϕ.

(a) Normal bed of 1000 μm glass beads in water.
(b) Inverse bed of 1000 μm plastic particles in water.